Solid State Ionics 320 (2018) 325–338

Contents lists available at ScienceDirect

Solid State Ionics

journal homepage: www.elsevier.com/locate/ssi

Preparation of Ni-metal oxide nanocomposites and their role in enhancing the electro-catalytic activity towards methanol and ethanol

H.B. Hassan*, Reham H. Tammam*

Faculty of Science, Department of Chemistry, Cairo University, PO 12613 Giza, Egypt

ARTICLE INFO

Keywords:
Methanol
Ethanol
Electrooxidation
Nanocomposite
EIS
Electrocatalysis

ABSTRACT

Ni–metal oxide (Fe_2O_3, ZnO, Co_3O_4 and MnO_2) nanocomposites were synthesized on carbon substrates by electrodeposition technique. These catalysts were tested as anodes for electrooxidation of both methanol and ethanol. To study the chemical composition of the deposits, energy dispersive X-ray spectroscopy (EDX) was used and the maximum wt% of metal oxides in the prepared composites was found to be 11.4, 11.7, 9.3 and 3.8 for Fe_2O_3, ZnO, MnO_2 and Co_3O_4, respectively. The morphology of the catalysts surface is significantly affected by the existence of metal oxides as confirmed by scanning electron microscope (SEM) images. The phase structure and the particle size of the catalysts were recognized from X-ray diffraction (XRD). A reduction in the Ni grains was seen in the matrix of the composites compared with that of Ni/C. Cyclic voltammetry (CV), chronoamperometry (CA) and electrochemical impedance spectroscopy (EIS) were employed to study the electrocatalytic activity of the prepared nanocomposites. All the results displayed a satisfactory electrocatalytic activity, better stability, lower charge transfer resistance, and stronger resistance to the poisoning of the nanocomposites compared with that of Ni/C. A synergistic effect among multiple active sites due to the presence of mixed oxides for the nanocomposites could enhance their electrocatalytic activity. The performance of the different prepared catalysts towards the electrooxidation process was established in the order of: Ni–Fe_2O_3/C > Ni–ZnO/C > Ni–Co_3O_4/C > Ni–MnO_2/C > Ni/C. Ni–metal oxide nanocomposites appeared to be promising and less expensive anode catalysts for fuel cell applications.

1. Introduction

The lack of natural energy resources is a real challenge for the modern life. Efforts are being made to find new energy resources that can supply human needs. Nowadays, other alternative fuels such as non-fossil Syngas (H_2/CO) is used, it is a very valuable and versatile energy carrier because it can be converted into liquid fuels. It is considered a renewable source of energy and it can be produced by electrochemical CO_2 reduction in an ionic liquid [1]. In addition, some alcohols like methanol and ethanol are being used as renewable fuels. It is known that the electrochemical power sources, for instance, fuel cells have been developed and used in a variety of life applications such as domestic and public transportation. Direct methanol or ethanol fuel cells are promising systems. Chemical energy of methanol or ethanol fuel is converted to electricity efficiently without combustion [2]. However, there are some limitations restrict the use of fuel cells at a commercial level. This is attributed to the high-cost materials used to design the fuel cell, particularly Pt catalyst that used as anodes especially in acid media [3–8]. Attempts have been employed to change Pt by some cheap materials as electrocatalysts for methanol and ethanol electrooxidation particularly in alkaline media [9–12].

For many years, nanocomposite electrodes have attracted interest because they are feasible to be prepared by properly incorporating nano-particulate to be co-deposited in the metal matrix through chemical or electrochemical methods. Moreover, they exhibited remarkable and technologically attractive properties due to their extremely fine microstructure and higher surface area. They exhibited higher catalytic activity towards the electrooxidation processes. Meanwhile, nanocomposites appeared to be promising and less expensive anode catalysts for fuel cell applications [13]. Some composites containing metal oxides (CeO_2, TiO_2, ZrO_2 and MoO_2) were used as anodes as they were more useful than Pt and less expensive. It was mentioned that metal oxides can supply OH^- species which induce oxidation/reduction process between different oxidation states of nanocomposite metal oxides to improve the catalytic efficiency [14]. Furthermore, CeO_2–ZrO_2 mixed oxides have been extensively used as oxygen storage components. It is noteworthy that cerium oxide may make CO-like species oxidated to prevent the catalyst deactivation [15]. Also, a

* Corresponding authors.
E-mail addresses: Hanaa@cu.edu.eg (H.B. Hassan), reham_tammam@cu.edu.eg (R.H. Tammam).

https://doi.org/10.1016/j.ssi.2018.03.020
Received 20 January 2018; Received in revised form 3 March 2018; Accepted 18 March 2018

platinum catalyst supported on a double oxide nanocomposite of tin oxide clusters and carbon-doped titanium dioxide nanocoatings on carbon nanotubes is used for electrooxidation of methanol. It leads to a much lower onset potential for the adsorbed CO oxidation with a much enhanced bifunctional effect in tin oxide [16]. Moreover, various metal oxides, for example, CeO_2, MnO_x, NiO, Co_3O_4 and their hydroxide analogues were found to be active materials for the electrocatalytic applications [17–22]. It was observed that inclusion of small amounts of metal oxides in addition to the active redox properties can help for developing the Pt electrocatalysts for fuel cells [23–26]. Also, cobaltous oxide deposited on a Pt electrode, shows prominent electrocatalytic activity towards the mediated electrooxidation of glucose and methanol [27]. The electrocatalytic activity of nano-CoO_x and MWNT composite modified GCE (CoO_x-MWNT/GCE) has been examined towards the oxygen evolution reaction (OER) by linear sweep voltammetry [28]. The addition of nickel oxide into both Pt/C and Pd/C catalysts could improve the methanol oxidation performance in terms of poisoning resistance and the reaction activity [10]. Moreover, SnO_2 promotes PtRu catalyst towards ethanol oxidation and it shows a lower onset potential and larger current density. Also, it could activate ethanol chemisorptions and increase the electroactive surface area, together with a faster intrinsic activity at lower overpotential [29]. It was previously seen that Pd/Cu_2O/MWCNT catalyst can be used as an excellent anode catalyst for ethanol electrooxidation in alkaline solution. The occurrence of Cu_2O increases the stability and CO poisoning tolerance of the Pd towards electrooxidation of ethanol [30]. Among various different metal oxides are MgO [31], NiO [32,33], MnO_2 [34], SnO_2 [35,36], CeO_2 [37], Mn_3O_4 and Co_3O_4 were used with Pd as a catalyst for fuel cells.

Ni-based catalysts like Ni–metal oxide nanocomposites have attracted importance in a wide range of fundamental researches and technological applications, for example; electrocatalysis and fuel cells [33,38–43]. This is due to the good distribution of the Ni particles and the high active surface area which lead to enhancement of the catalytic activity towards the electrooxidation processes. Ni–metal oxide nanocomposites are synthesized by co-depositing metal oxides like ZnO, Cr_2O_3, MgO or TiO_2 in the Ni-plated layer under the electric field [38,39,44–47]. Moreover, the rate of oxide particle co-deposition depends on many factors such as size, shape, charge, current density, temperature, pH and time. Their applications as anode catalysts were estimated towards electrooxidation of relatively low molecular mass alcohols in alkaline fuel cells [48,49]. Their catalytic activity is attributed to the formation of a higher valence Ni oxide which acts as chemical oxidizing agent [50]. An enhancement of the durability and catalytic activity is achieved when using these composite materials as electrocatalysts [51,52]. It was seen that Ni–MgO composite exhibits low overvoltage for alcohol oxidation, acts as effective anode materials with higher efficiency, increases the anti-poisoning ability of the Ni catalysts and improves the kinetic processes [40,53–55]. Also, the existence of TiO_2 co-deposited within the Ni matrix as a nanocomposite increases its electrocatalytic activity [38,39]. Moreover, nickel modified with MnO_x is significantly active for the methanol electrooxidation [54]. Effective electrocatalysts for oxygen reduction reaction (ORR) was carried by using transition metal oxides [56–58]. This is due to the multiplicity of the active sites which may be responsible for the improvement of ORR activities. Additionally, Ni–NiO@C nanocomposites showed a high electrocatalytic activity for methanol oxidation [59].

Accordingly, the main goal of this work is to develop Ni-based nanocomposites for methanol and ethanol electrooxidation. Ni–metal oxides (Fe_2O_3, ZnO, Co_3O_4 and MnO_2) nanocomposites were synthesized on carbon electrodes using a simple electrodeposition technique. The prepared electrodes will be used as anodes for alcohols electrooxidation. It is anticipated to improve the catalytic activity of the Ni and find reasonable explanations for the effect of metal oxides in enhancing the electrooxidation process.

2. Experimental techniques

2.1. Synthesis of Ni–metal oxide nanocomposites

For the synthesis of the Ni–metal oxide nanocomposite working electrodes, carbon substrates were used for the electrodeposition process, each of a geometrical electrode area of 0.125 cm^2. The carbon electrodes were cleaned mechanically using metallurgical papers of various grades, then they were soaked in acetone, rinsed with double distilled water and finally dried. The electrode surface area was calculated from the geometrical area and the current density value was referred to it. Ni Watts` bath was utilized for the deposition of Ni and Ni–metal oxide nanocomposites, it has the composition of: 240 g l^{-1} nickel sulphate, 45 g l^{-1} nickel chloride and 30 g l^{-1} boric acid, operated at pH 5, 55 °C, 150 rpm and 40 mA cm^{-2} for 30 min in the absence and presence of different concentrations (1–12) g l^{-1} of each metal oxide. Before the electrodeposition of composites, the oxide particles were stirred in the electrolyte solution by using a magnetic stirrer to achieve a uniform suspension of particles and break down the agglomeration. Ethanol and methanol were used without purification. Triple distilled water was used for the solutions preparation. Chemicals used were Sigma-Aldrich products of analytical grade and used without any further purification.

2.2. Electrochemical measurements

The electrochemical techniques were done in a conventional three-electrode system. The working electrode was Ni/C or Ni–metal oxide nanocomposites, the reference electrode to which all potentials were referred is the Hg/HgO/1.0 M NaOH (MMO), and a Pt sheet was used as a counter electrode. Measurements were done in an aerated 1.0 M NaOH at room temperature of 25 ± 0.2 °C. The electrochemical measurements were performed by cyclic voltammetric and chronoamperometric techniques using Amel 5000 (supplied by Amel Instrument, Italy) driven by an IBM PC for data processing. The PC was interfaced with the instrument through a serial RS–232 card. To control the Amel 5000 system, Amel easyscan software was used and connected to PC. The electrochemical impedance spectroscopy (EIS) data was measured at frequencies ranging from 100 kHz to 10 MHz at 10 mV amplitude. Zahner Elektrik Meβtechnik, IM6, Germany, was used to perform the EIS and the experimental impedance spectra were fitted with the equivalent circuits included with the IM6 package using the “SIM” program. The suitability of the elements in the proposed equivalent circuits to fit the experimental data was judged by the error 1.5% of the fitting and by comparing the calculated and the experimental impedance plots.

2.3. Surface analysis techniques

Scanning electron microscopy Model Quanta 250 FEG (Field Emission Gun) attached with EDX unit (Energy dispersive X–ray analyses), with accelerating voltage 30 KV (FEI Company, The Netherlands) was applied to investigate both the chemical composition and the surface morphology of the prepared nanocomposites. X-ray diffractometer (XRD, Rigaka, Japan) with CuK_α (λ = 1.540 Å) was used to study the crystal structure and particle size of the prepared catalysts. It is operated at 45 kV and 40 mA. The step scanning size, range and rate were 0.02°, 10°–100°, and 0.05°/s, respectively.

The values of zeta potential for each metal oxide particles (Fe_2O_3, ZnO, Co_3O_4 and MnO_2) was measured using a laser zeta meter (Zetasizer 2000, Malvern Instruments, UK). A sample powder of every metal oxide (about 0.02 g) was placed into ≈50 ml of Ni Watts' solution and the sample was stirred for 50 min at pH 5, after that the measurement of zeta potential was done. Actual surface areas of the prepared catalysts were measured using Nova 2000 series based on the well-known Brunauer, Emmett and Teller (B.E.T.) theory.

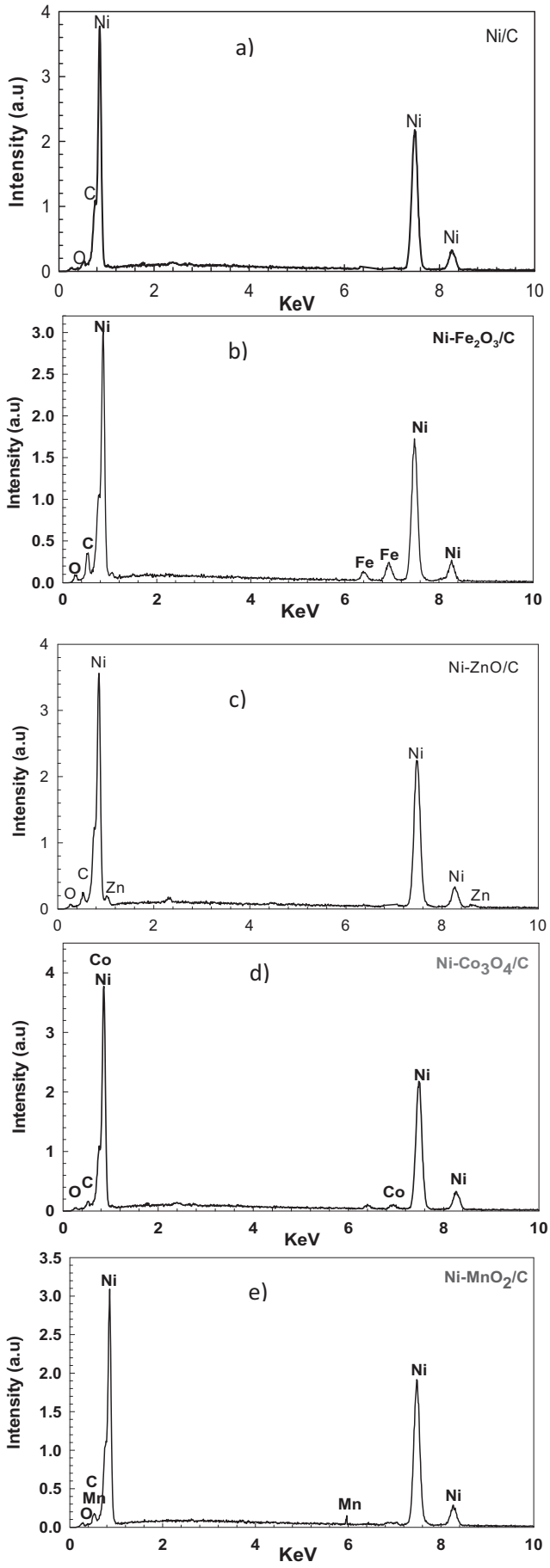

Fig. 1. EDX analysis of (a) Ni/C, (b) Ni–Fe_2O_3/C, (c) Ni–ZnO/C, (d) Ni–Co_3O_4/C and (e) Ni–MnO_2/C catalysts prepared by electrodeposition at 40 mA cm^{-2} for 30 min.

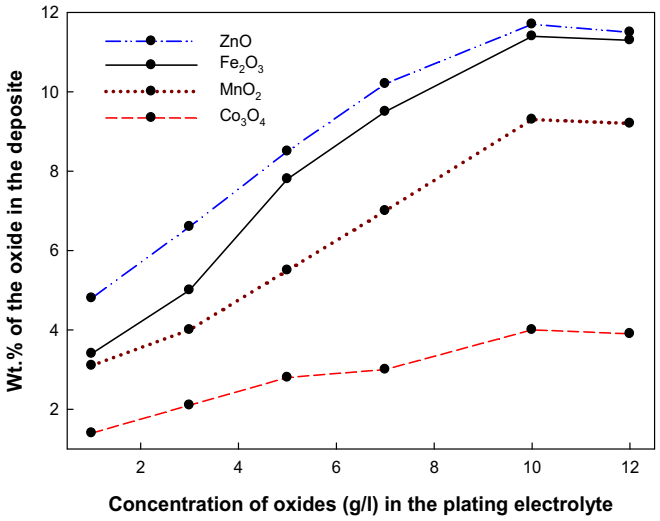

Fig. 2. Variation of wt% of metal oxides in the deposits with its concentration in the deposition electrolyte.

3. Results and discussion

3.1. Surface characterization of nanocomposites

Electrodeposition technique was employed to synthesis Ni and Ni–metal oxide (Fe_2O_3, ZnO, Co_3O_4 and MnO_2) nanocomposites on carbon substrates from Ni Watts' bath at the optimum conditions as was mentioned in the Experimental techniques section. The most favorable conditions were determined from our previous work on similar Ni composites [38–40]. The surface composition of each electrode was investigated by energy dispersive X-ray spectroscopy (EDX) and the quantity of each metal oxide deposited within the Ni layer was estimated and the results are presented in Figs. 1 and 2. Characteristic peaks for Ni, O, and C were seen in the EDX spectrums for the Ni/C and Ni–metal oxide composite electrodes (Fig. 1a–e), while additional peaks for Fe, Zn, Co and Mn were observed for the Ni–metal oxide composite electrodes (Fig. 1b–e). By inspecting Fig. 2, it is clear that the weight percentage (wt%) for the studied metal oxides increases with increasing its concentration in the plating electrolyte reaching its maximum wt% at a concentration of 10 g l^{-1}. However, any further increase in the concentration of metal oxides in the plating electrolyte beyond 10 g l^{-1} has a slight effect on the incorporation process and this indicated that the co-deposition of the metal oxides in the Ni matrix reached its saturation level [60]. The mechanism of the co-deposition of metal oxides within the Ni matrix depends on the adsorption phenomena and this was explained by Guglielmi's two-step adsorption model [61]. A comprehensive explanation of this model was discussed in the literature [38–40,62–64]. The zeta potential of each metal oxide is a significant factor in the co-deposition process. All the studied metal oxides have negative zeta potentials at the operating pH 5, their values were −20, −22, −18, −15 mV for Fe_2O_3, ZnO, Co_3O_4 and MnO_2, respectively. This could help the Ni^{2+} adsorption on the metal oxides surface and consequently it will facilitate the co-deposition process. Moreover, as the metal oxides concentration in the plating electrolyte increases, the amount of adsorbed Ni^{2+} on the surfaces of metal oxides increases and they will be together transmitted to the cathode surface to be deposited under the effect of the applied electric field [65]. As a result, an increase in the wt% of the metal oxides deposited in the deposited layer is observed (Fig. 2). The maximum amount of the metal oxides co-deposited within the nickel matrix was obtained at a concentration of

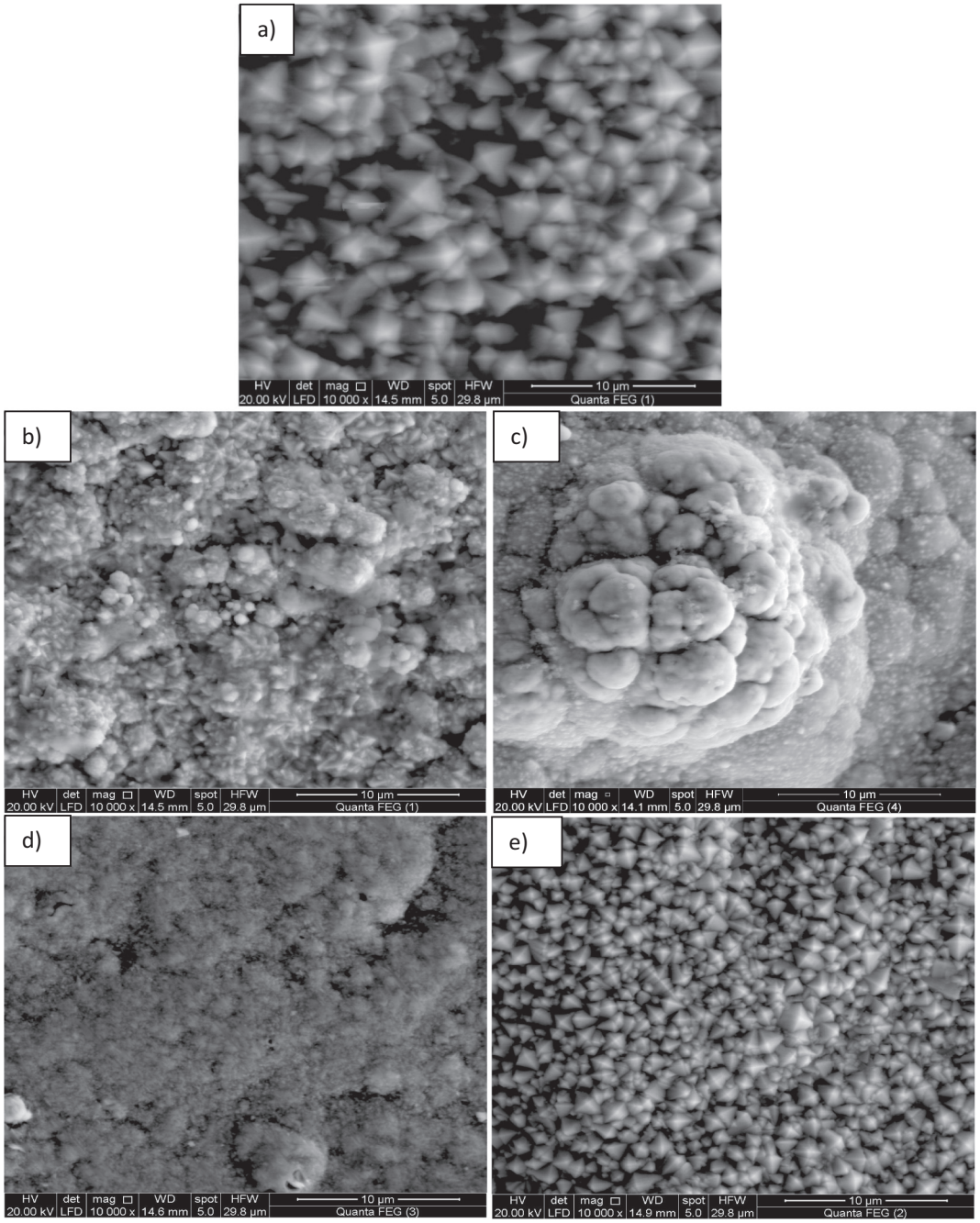

Fig. 3. SEM images of (a) Ni/C, (b) Ni–Fe_2O_3/C, (c) Ni–ZnO/C, (d) Ni–Co_3O_4/C and (e) Ni–MnO_2/C catalysts prepared by electrodeposition at 40 mA cm^{-2} for 30 min.

10 g l^{-1} for each metal oxide. The maximum wt% of the metal oxides deposited in the Ni matrix was found to be 11.3, 11.7, 9.3 and 3.8 for Fe_2O_3, ZnO, MnO_2 and Co_3O_4, respectively.

Fig. 3 displayed the SEM images of Ni/C and Ni–metal oxides (Fe_2O_3, ZnO, Co_3O_4 and MnO_2) nanocomposites deposited on carbon substrates at a constant current density of 40 mA cm^{-2}, pH 5, 150 rpm and temperature 55 °C in the absence and presence of 10 g l^{-1} of each metal oxide. SEM micrograph of the electrodeposited Ni/C electrode (Fig. 3a) demonstrated a regular pyramidal structure of Ni crystallites with a relatively greater Ni grains in contrast to the other Ni composites. The co-deposition of metal oxide particles in the Ni deposits induced some changes in the morphology of the resulting composites as shown in Fig. 3b–e. Actually, a relatively good dispersion of Ni particles on the carbon substrate was observed for the composite electrodes with a reduction in the Ni grain size depending on the characteristics of each metal oxide. This is due to the distribution metal oxide particles on the boundaries of Ni grains, which inhibits its growth and results in a fine surface [66].

On the other hand, the phase structure of Ni/C and Ni–metal oxide composites was studied by XRD (Fig. 4). The XRD pattern for Ni/C electrode (Fig. 4a) showed three characteristic diffraction peaks at 44.5°, 51.8°, and 76.3°, which corresponded to the (111), (200), and (220) planes of crystalline Ni, respectively. While, XRD patterns of the Ni–metal oxide composites displayed the same diffraction peaks of Ni but with relatively lower intensities, in addition to other small peaks hardly detected by the naked eye and observed at different angles can be assigned to the different metal oxides as shown in Fig. 4b–e. XRD pattern of Ni–Fe_2O_3/C composite electrode (Fig. 4b) shows some characteristic peaks of lower intensities for Fe_2O_3, present at 2θ of 33.4° (104), 36.0° (110), 41.2° (113), 49.8° (024) and 54.4° (116), in addition

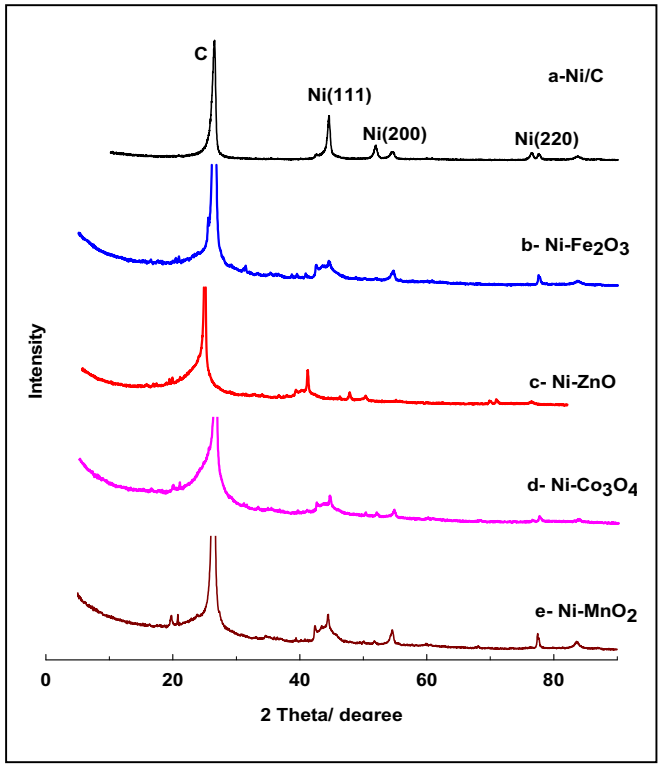

Fig. 4. XRD patterns of (a) Ni/C, (b) Ni–Fe_2O_3/C, (c) Ni–ZnO/C, (d) Ni–Co_3O_4/C and (e) Ni–MnO_2/C catalysts prepared by electrodeposition at 40 mA cm^{-2} for 30 min.

to the diffraction peaks of Ni that mentioned above but with lower intensities indicating a very small particle size of Ni in the composite sample. On the other side, XRD pattern of Ni–ZnO/C (Fig. 4c) indicates some diffraction peaks of lower intensities present at 2θ of 31.7° (100), 34.4° (002), 36.2° (101), 47.4° (102), 56.6° (110), 62.8° (103) and 69.1° (201) were assigned to ZnO, besides the diffraction peaks of Ni. The Ni–Co_3O_4/C electrode (Fig. 4d) shows characteristic peaks present at 2θ of 19.0° (111), 31.3° (220), 36.85° (331), 38.5° (222), 44.8° (440), 56.7° (422), 59.4° (511) crystal planes due to the Co_3O_4 in addition to the diffraction peaks of Ni. Fig. 4e indicates some diffraction peaks for MnO_2 appeared at 2θ of 37.4° (400), and 60.2° (002), respectively, are assigned to MnO_2, and the other peaks should be ascribed to the characteristic peaks for Ni but with lower intensities.

Based on XRD and SEM results, it can be claimed that the existence of metal oxides such as Fe_2O_3, ZnO, Co_3O_4 and MnO_2 modified the surface morphology and reduced the size of Ni grains. The average particle sizes of Ni grains are calculated from XRD data based on Scherrer's formula [67] and the results are presented in Table 1. The average particle sizes of Ni grains were found in the order of: Ni–Co_3O_4 < Ni–ZnO < Ni–Fe_2O_3 < Ni–MnO_2 < Ni/C (see Table 1).

Table 1
The average Ni particle size of different electrodes as calculated from XRD data, the actual surface area, the oxidation current density values for methanol and ethanol at +1.0 V (MMO), and the efficiency after 50 cycles (I_{p50}/I_{p1} ×100).

Electrode	Ni particle size (nm)	Actual surface area m^2/g	I_p, mA cm^{-2} for 1.0 M MeOH	Efficiency after 50 cycles for MeOH	I_p, mA cm^{-2} for 1.0 M EtOH	Efficiency after 50 cycles for EtOH
Ni/C	100	33	64	72 %	46	67 %
Ni-MnO_2/C	90	92	78	73 %	83	71 %
Ni-Co_3O_4/C	65	101	137	76 %	134	74 %
Ni-ZnO/C	70	133	200	83 %	170	81 %
Ni-Fe_2O_3/C	72	155	339	93 %	302	89 %

Also, the actual surface area of each catalyst was calculated and the results were reported in Table 1. The real surface areas were found in the order of Ni/C < Ni–MnO_2 < Ni–Co_3O_4 < Ni–ZnO < Ni–Fe_2O_3.

3.2. Electrocatalytic performance of nanocomposites

The electrochemical catalytic activities of the prepared Ni/C and Ni–metal oxide nanocomposites were investigated in 1.0 M NaOH solutions using the cyclic voltammetric technique. The results are shown in Figs. 5–7 in the absence and presence of 1.0 M methanol and 1.0 M ethanol. All the catalysts prepared at the experimental conditions of 40 mA cm^{-2}, pH 5, 150 rpm and temperature of 55 °C in the absence and presence of 10 g l^{-1} of each metal oxide. The cyclic voltammograms were measured in a potential range from −0.5 up to +1.2 V (MMO) in the anodic, then in the cathodic direction at a scan rate of 50 mV s^{-1}. Obviously, two pairs of well–defined redox peaks due to the Ni redox species (Ni^{3+}/Ni^{2+}) were observed in the cyclic voltammogram at +0.46 and +0.29 V (MMO) in the positive and negative direction, respectively for Ni/C electrode (Fig. 5a). The anodic peak is due to oxidation of $Ni(OH)_2$ to NiOOH and the cathodic peak is due to the reduction of NiOOH to $Ni(OH)_2$ as mentioned in the literature [48,68], due to the following reaction:

$$Ni(OH)_2 + OH^- = NiOOH + H_2O + e^- \quad (1)$$

While, for the Ni–metal oxide nanocomposites (Fig. 5b), the redox peaks of Ni appeared at potentials of +0.59, +0.54, +0.53 and +0.57 V (MMO) for Ni–Fe_2O_3/C, Ni–ZnO/C, Ni–Co_3O_4/C and Ni–MnO_2/C, respectively in the anodic direction, and at +0.33, +0.34, +0.34 and +0.40 V (MMO), respectively in the cathodic direction but with different catalytic activities. It was observed that the anodic peaks are to some extent shifted to the positive direction and the cathodic peaks are shifted towards the less negative direction depending on the metal oxides. But the values of current densities for the redox peaks are much higher in Ni–metal oxide nanocomposites compared with that obtained with Ni/C. Furthermore, the best performance was found for Ni–Fe_2O_3/C, its catalytic activity was 3 times larger than that of Ni/C, then Ni–ZnO/C electrode, its performance is about 1.7 times higher than that of Ni/C. The relatively small performance was recorded for Ni–Co_3O_4/C and Ni–MnO_2/C, but their performances are still higher than that of Ni/C. From the cyclic voltammograms (Fig. 5b), it is clear that the presence of metal oxides such as Fe_2O_3, ZnO, Co_3O_4 and MnO_2 enhances the formation of Ni^{3+}/Ni^{2+} redox species and the formation of Ni^{3+} species is essential for alcohols oxidation process [69–71]. The current density of the redox peaks and the catalytic activity were found in the order of Ni–Fe_2O_3 > Ni–ZnO > Ni–Co_3O_4 > Ni–MnO_2 > Ni/C. From this order, it can be concluded that a higher catalytic activity is connected with a small Ni grain size and thus a higher active surface area of the prepared catalyst. Moreover, the relatively high redox current for the nanocomposite electrodes in comparison to Ni/C electrode could due to the presence of multiple electrochemical activity sites [72]. Also, the peak to peak separation potential (ΔE_p) for the composite electrodes shows an approximate reversible system which value is ~0.21–0.17 V (MMO) and this indicated that a rapid electron transfer could occur between the composite electrode surfaces and the electrolyte [73–76].

Cyclic voltammetric curves at a scan rate of 50 mV s^{-1} for 1.0 M methanol and 1.0 M ethanol in 1.0 M NaOH were measured at the different prepared electrodes and the results are shown in Figs. 6 and 7, respectively. A single anodic peak is observed corresponding to the oxidation of methanol (Fig. 6) and ethanol (Fig. 7) for all the studied electrodes but with different current densities. The oxidation current density gradually increases at the starts at a potential corresponding to Ni^{3+} species formation, reaching its maximum as an oxidation peak. The anodic current increases as a result of alcohols oxidation is accompanied by a decrease in the cathodic current indicating that alcohol could lessen the entire high valence of nickel species formed. The

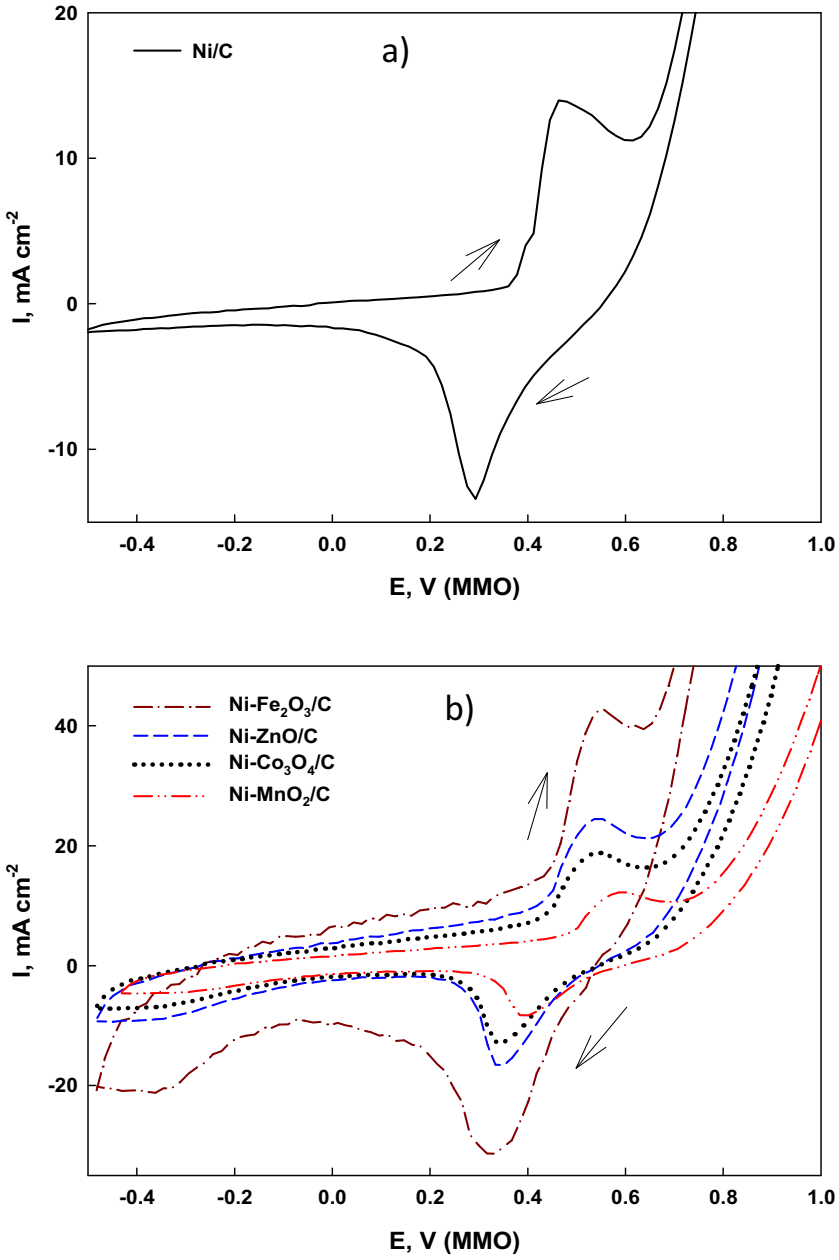

Fig. 5. Cyclic voltammograms of (a) Ni/C and (b) Ni–Fe_2O_3/C, Ni–ZnO/C, Ni–Co_3O_4/C and Ni–MnO_2/C catalysts in 1.0 M NaOH at a scan rate of 50 mV s^{-1}.

oxidation current densities of the different nanocomposites are calculated at a constant potential of +1.0 V (MMO) (see Table 1). From the data presented in Table 1, it can be concluded that Ni–Fe_2O_3/C has the highest catalytic activity as it has the highest oxidation current density. Also, the order of decreasing the catalytic activity of the proposed catalysts towards methanol and ethanol oxidation was found in the order of Ni–Fe_2O_3 > Ni–ZnO > Ni–Co_3O_4 > Ni–MnO_2 > Ni/C and the onset potential of oxidation shifted to more negative values in the same order. The oxidation of alcohol may due to the proposed involvement of Ni^{3+}/Ni^{2+} surface species [77]. When NiOOH is formed, methanol or ethanol oxidation starts at the potential of NiOOH formation, as indicated by the following reaction:

$$NiOOH + alcohol \rightarrow Ni(OH)_2 + intermediate\ products \quad (2)$$

This mechanism was reported by Fleischmann et al. [78], where alcohols and organic compounds were oxidized at a potential that agreed precisely at which NiOOH was created. Methanol or ethanol is oxidized by the reduction of NiOOH to $Ni(OH)_2$ with the development of intermediate products. Likewise, it is expected to get a cyclic voltammogram free from the NiOOH reduction peak in the cathodic range (see Figs. 6 and 7).

The excellent catalytic activity inherited with the nanocomposite electrodes could due to the presence of more than one type of the metal oxides compared with that of Ni/C. A synergism between the different oxides could lead to a higher adsorbability of methanol or ethanol on the nanocomposite surface [79]. It is most significant that both the redox current obtained in the blank solution (1.0 M NaOH) and the oxidation current of methanol and ethanol obtained with the nanocomposites are higher, likely caused by an increase in the electroactive area of the anode owing to the smaller Ni particle sizes in the composites compared with that of Ni/C. So, methanol or ethanol is predictable to be adsorbed rather easily on the composite surfaces. Moreover, the presence of different metal oxides such as Fe_2O_3, ZnO, Co_3O_4 and MnO_2 play a significant role in the formation of NiOOH species, Ni^{2+} can be oxidized to Ni^{3+} by the strong oxidant higher valence metal oxides leading to an increase in the Ni^{3+} concentration in the matrix. As a

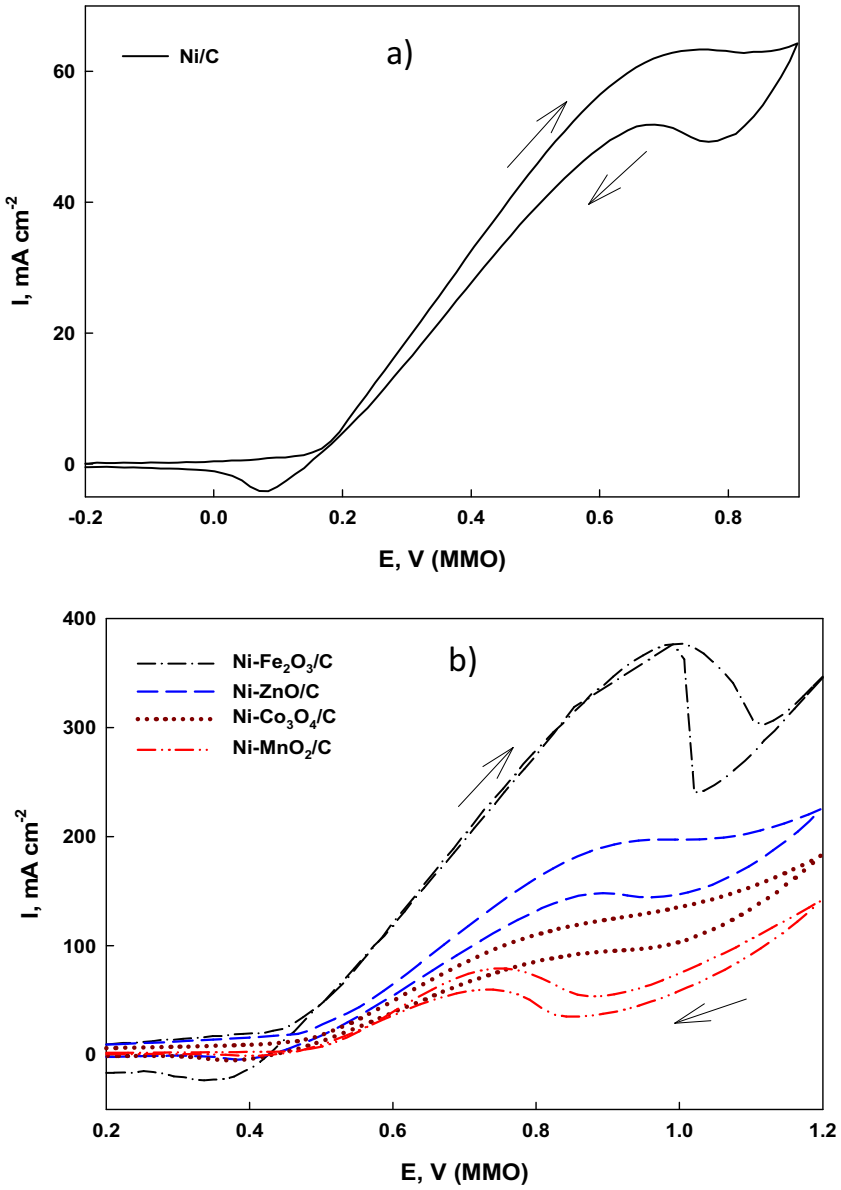

Fig. 6. Cyclic voltammograms of (a) Ni/C and (b) Ni–Fe_2O_3/C, Ni–ZnO/C, Ni–Co_3O_4/C and Ni–MnO_2/C catalysts in 1.0 M NaOH + 1.0 M MeOH at a scan rate of 50 mV s^{-1}.

consequence, an increase in the conductivity of the matrix occurs which enhances both methanol and ethanol oxidation [80]. On the other side, the catalytic participation of some higher valent states of metal oxides in electron transfer relay is speculated [81]. The existence of more than one metal oxide on the carbon electrode surface could act as a good mediator for electron transfer in electrooxidation of methanol and ethanol [82]. For example, electrochemical oxidation of Fe(III) to Fe (VI) of Ni–Fe_2O_3/C nanocomposite electrode, in a strong alkaline solution is possible. Moreover, species such as Fe(IV), Fe(V), or Fe(VI) may exist in less alkaline media at the iron oxide solid/aqueous solution interface and Fe(IV) surface species is highly reactive [83]. These higher valence species could enhance the formation of Ni^{3+} species and help in the oxidation of methanol and ethanol by a direct or indirect way. Moreover, the improved catalytic activity inherited to Ni–ZnO/C electrode is due to the reaction of ZnO with NaOH to give $Zn(OH)_2$ which dissolve in a strong alkaline solution to give zincates [84,85], and these species could enhance the oxidation of Ni^{2+} to Ni^{3+} as well as it could enhance the oxidation of alcohol. On the other hand, OH^- species are employed in the electrochemical redox reaction of Co_3O_4 for the Ni–Co_3O_4/C nanocomposite electrode. Co_3O_4 can be converted to CoOOH, and CoOOH is converted to CoO_2 [86]. The reactions can be expressed as:

$$Co_3O_4 + OH^- + H_2O \leftrightarrow 3CoOOH + e^- \quad (3)$$

and

$$CoOOH + OH^- \leftrightarrow CoO_2 + H_2O + e^- \quad (4)$$

The catalytic property of this electrode in the alkaline solution was related to CoOOH, CoO_2 and NiOOH. Therefore, methanol or ethanol could be also oxidized by the active catalyst of Co^{3+}, Co^{4+} and Ni^{3+} moieties. It is likely that the existence of MnO_2 in the Ni–MnO_2/C electrode could increase Ni^{3+} content. Mn^{4+} species can be converted during the anodic scan to the powerful and unstable oxidant Mn^{5+}, which can convert some of the Ni^{2+} to Ni^{3+} and cause an increase in the conductivity of the former according to the following reaction [80,87]:

$$Mn^{5+} + Ni^{2+} \rightarrow Ni^{3+} + Mn^{4+} \quad (5)$$

On the other hand, some authors [80,87] claimed that the electrooxidation process proceeds via Mn^{4+} as the following reaction:

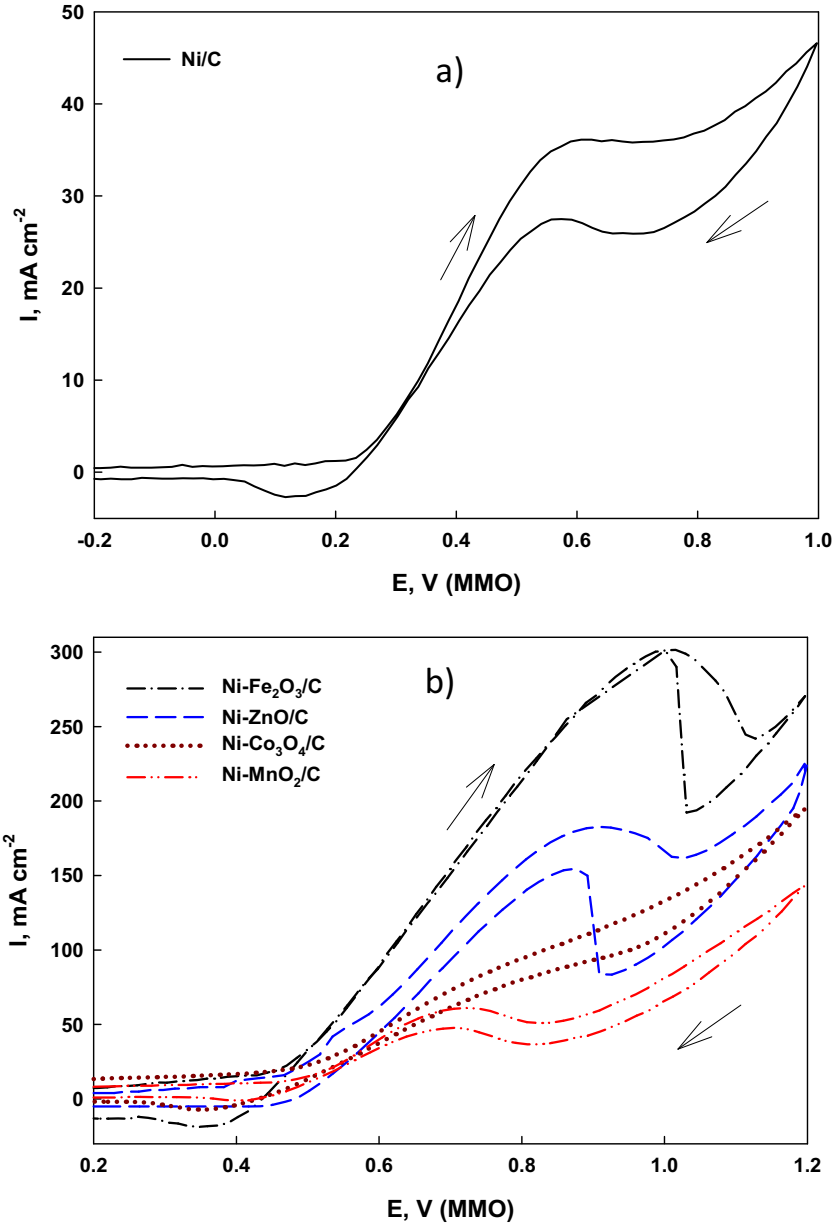

Fig. 7. Cyclic voltammograms of (a) Ni/C and (b) Ni–Fe_2O_3/C, Ni–ZnO/C, Ni–Co_3O_4/C and Ni–MnO_2/C catalysts in 1.0 M NaOH + 1.0 M EtOH at a scan rate of 50 mV s^{-1}.

Mn^{4+} + methanol or ethanol ↔ oxidation product + Mn^{3+} (6)

A dual role could be exerted by the mixed oxides in the Ni–metal oxide nanocomposite electrodes; one enhances the adsorption of alcohol and the other causes mediation of the oxidation process.

Moreover, Fig. 8a, b illustrates the relation between the anodic peak current density and the concentration of methanol and ethanol, respectively at Ni/C and the nanocomposite electrodes. It is clear that the anodic peak current density in the positive scan increases linearly as the bulk concentrations of methanol and ethanol increase and the linear dynamic range (LDR) is found from 0.05 to 2.0 M, while at higher concentration beyond 2.0 M the linearity is no longer present.

On the other side, Fig. 8c, d displays the chronoamperometric analysis for the synthesized catalysts in the presence of 1.0 M methanol (Fig. 8c) and 1.0 M ethanol (Fig. 8d) obtained at +1.0 V (MMO). It is clear that all samples showed some current decay at the first seconds before the relative steady state is attained. The decay is probably attributed to the adsorption of some incomplete oxidation products on the carbon electrode surface [88]. Moreover, the starting decrease can be attributed to fast methanol or ethanol molecules oxidation near to the electrode surface. Afterwards, the kinetic of methanol or ethanol oxidation reaction changes to be under mass transfer–controlling process. The current densities obtained with the synthesized nanocomposites were considerably higher than that obtained with Ni/C. The metal oxides cause an increase in the adsorption ability of the hydroxyl ion onto the catalyst surface. Moreover, metal oxides could activate water, which can oxidize the adsorbed carbonaceous intermediate species and thereby liberate the active sites of the surface [75,76]. Ni–Fe_2O_3/C nanocomposite electrode shows the highest performance and stability towards either methanol or ethanol oxidation, also it maintains its catalytic activity for a relatively long time. Compared to the Ni/C, the higher I_f/I_b value (I_f and I_b are peak currents in the forward and backward, respectively) (see Figs. 6 and 7) of the nanocomposites indicates a higher anti-poison property as the I_f/I_b ratio reflects the tolerance ability to carbonaceous species accumulated [89]. On the other hand, the relatively poor catalytic activity and stability of the Ni–Co_3O_4/C and Ni–MnO_2/C compared to Ni–Fe_2O_3/C and Ni–ZnO/C electrocatalysts are related to the low solubility of Co_3O_4 and MnO_2 in

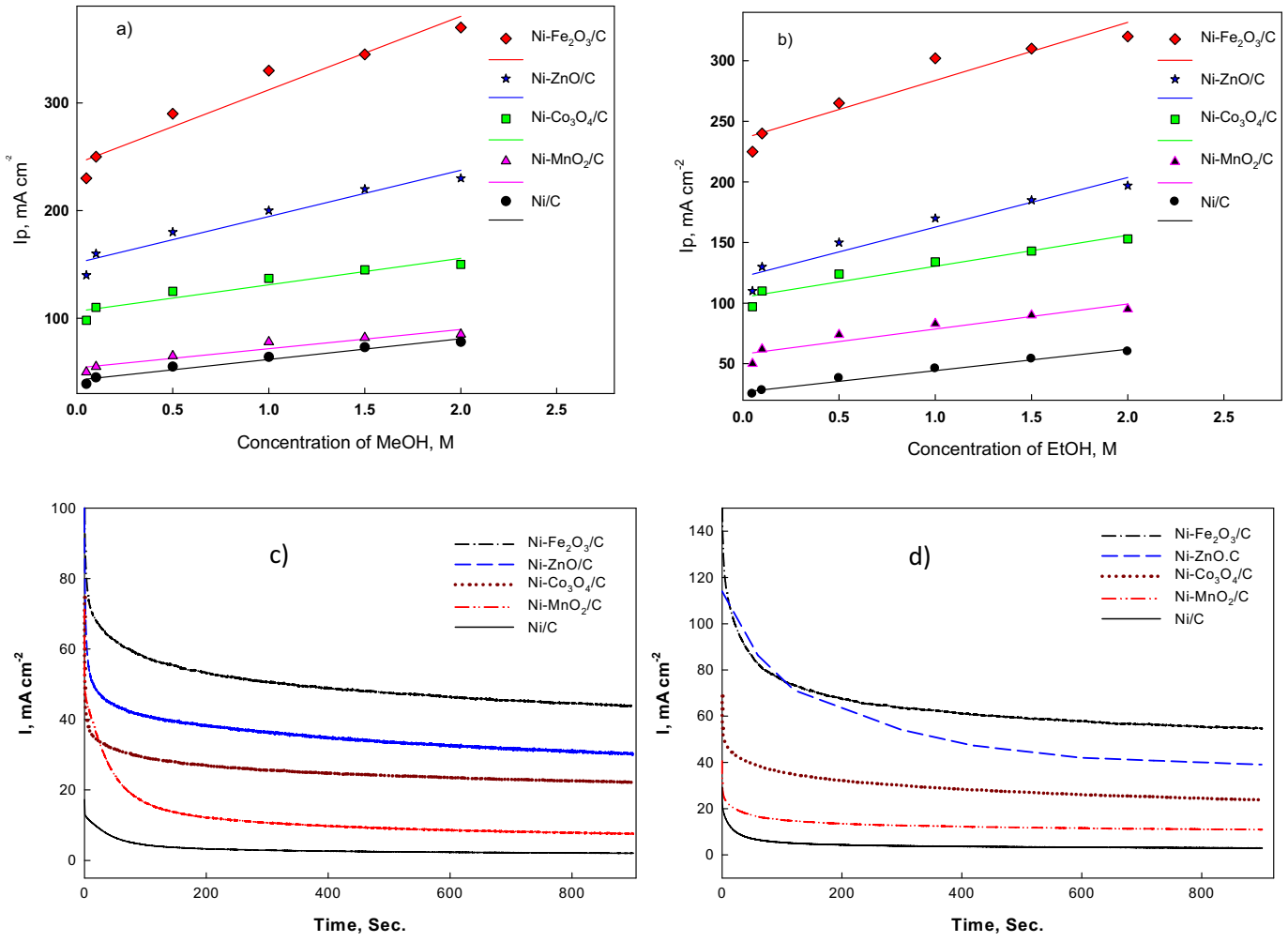

Fig. 8. a–d. Effect of different concentrations of a) methanol and b) ethanol on the oxidation peak current density at the prepared electrodes and chronoamperometric curves for the studied electrocatalysts at +1.0 (MMO) in the presence of (c) 1.0 M MeOH and (d) 1.0 M EtOH in 1.0 M NaOH solution at 25 °C.

the alkaline solutions [76]. But their stabilities and their catalytic activities are still larger than that of Ni/C. On the other hand, the stability of the prepared nanocomposites was investigated from the repeated cyclization and the efficiency of each catalyst after 50 cycles was calculated and reported in Table 1. Comparable results to those obtained from the chronoamperometric studies were obtained.

3.3. Electrochemical impedance spectroscopy (EIS)

EIS is a powerful technique used to investigate the kinetics of electrooxidation of small organic molecules in fuel cells [90,91]. To evaluate the electrocatalytic activity of the modified electrodes towards alcohols electrooxidation in terms of the charge transfer resistance [92], EIS measurements were carried out at a constant potential of +0.5 V (MMO). This potential is corresponding to the formation of Ni^{3+} for all the prepared electrodes. As previously seen, loading of metal oxides within the Ni matrix can effectively promote the catalytic activity of methanol or ethanol electrooxidation. Bode and Nyquist plots (Figs. 9, 10 and 11) were performed to further study the electrocatalytic performance of the synthesized Ni/C, Ni–Fe_2O_3/C, Ni–ZnO/C, Ni–Co_3O_4/C and Ni–MnO_2/C in 1.0 M NaOH solution in the absence and presence of 1.0 M methanol and 1.0 M ethanol. The impedance data are analyzed using the equivalent circuit shown in Fig. 12 in the blank and in methanol or ethanol solutions and the circuit elements are fitted [79]. The experimental data are shown by the symbols and the simulated data, which are generated using the equivalent circuit depicted in Fig. 12, are shown as solid lines. Good agreement between the simulated and experimental data is obtained with an average error of 1.5%. The equivalent circuit shown in Fig. 12 represents Randel's circuit with components corresponds to the presence of charge transfer resistance (R_{ct}) at the interface of electrode/electrolyte. Replacement of the capacitor C with a constant phase element (CPE) in the equivalent circuit is denoted as Q_{dl} in Table 2. This was due to a microscopic roughness which makes an inhomogeneous distribution in the capacitance of the double layer and in the solution resistance (R_s) [93]. The impedance of a constant phase element (Z_{CPE}) can be expressed as:

$$Z_{CPE} = [C(j\,\omega)^{\alpha}]^{-1} \quad (7)$$

where $-1 \le \alpha \le 1$, $j = (-1)^{1/2}$, $\omega = 2\pi f$, ω is the angular frequency in rad/s, f is the frequency in Hz = s^{-1} and α is a fitting parameter which is an empirical exponent varies from 1 for a perfect capacitor and 0 for a perfect resistor. As can be estimated from Table 2, the empirical exponent α was varied between 0.59 and 0.89, which confirmed the deviation from the behavior of ideal capacitive as a result of surface heterogeneity, roughness factor and adsorption effects [93]. This means that the studied metal oxide composites do not act as perfect capacitors. At potential (E = +0.5 V (MMO)), the methanol or ethanol oxidation is kinetically (charge–transfer) controlled (R_{ct} is obtained in Table 2). The outcomes were contrasted with that acquired for Ni/C electrode prepared under a similar experimental setting. The imaginary impedance (Z') is plotted against the real impedance (Z), in Nyquist plots for the examined electrodes at methanol or ethanol

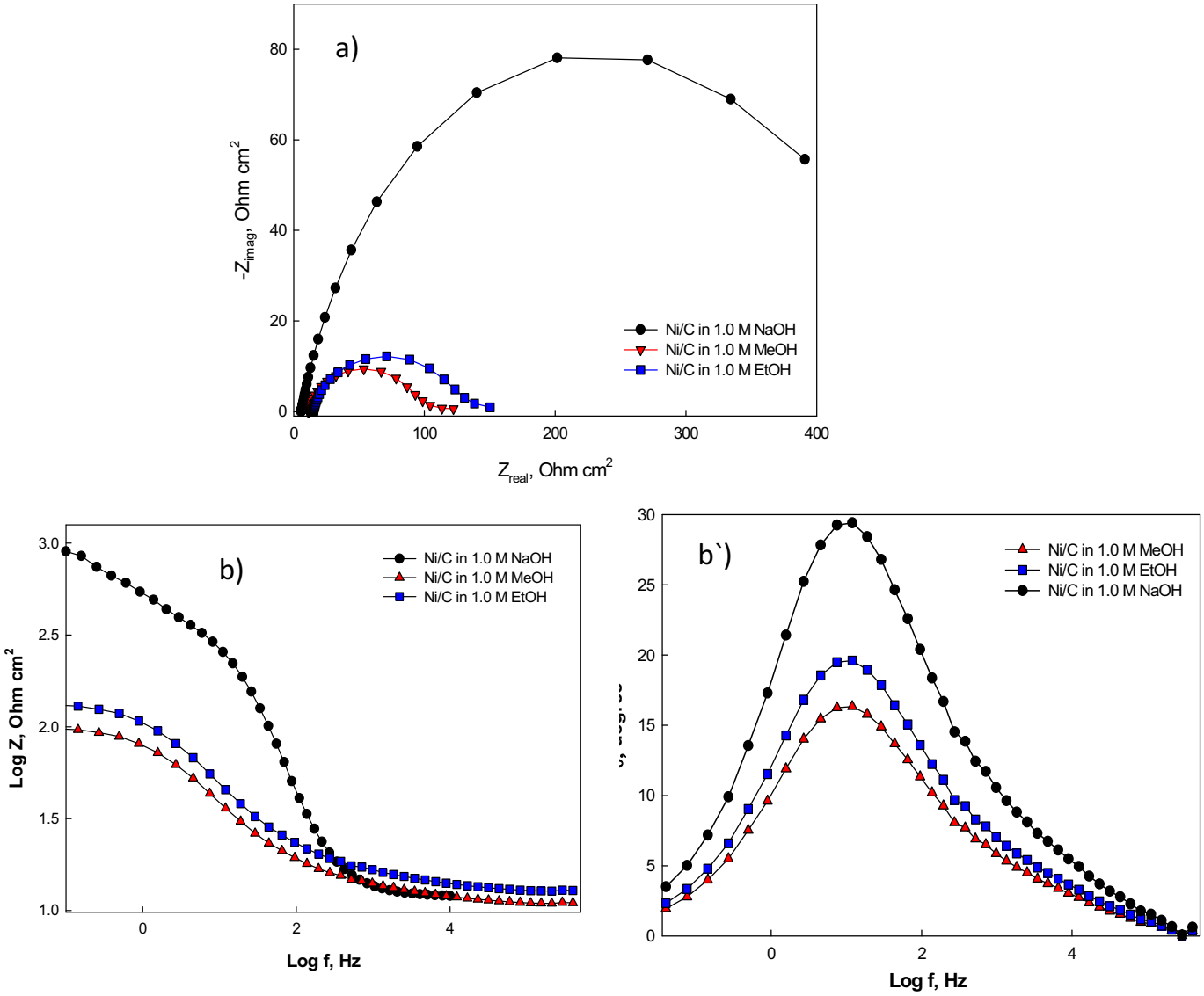

Fig. 9. Nyquist plots (a) and Bode plots (b, b′) of Ni/C electrocatalyst prepared at 40 mA cm^{-2} in 1.0 M NaOH, 1.0 M methanol in 1.0 M ethanol at +0.5 V (MMO) and 25 °C. Symbols denote experimental data, while the continuous lines represent the fitted data.

concentration of 1.0 M in 1.0 M NaOH as can be observed from Fig. 9a. A capacitive loop is seen which verify the faradic reaction (methanol or ethanol oxidation) with a diameter coordinated with the charge transfer resistance (R_{ct}) [95]. The capacitive loop appears to be higher in the blank solution (1.0 M NaOH) than in methanol or ethanol solution. For the Ni–Fe_2O_3/C the diameter of the semicircle was smaller than that of Ni/C which signifying that Ni–Fe_2O_3/C has a reduced resistance and makes large electron transfer efficiency. The resultant Nyquist plots were illustrated in Fig. 10 in the absence and presence of 1.0 M methanol or 1.0 M ethanol, it is clear that the highest diameter of semicircle was found for Ni/C, while Ni–Fe_2O_3/C had the most shrunk diameter among the different studied electrocatalysts. This could due to the good conductivity and the higher its active surface area [93]. This means that during methanol or ethanol electrooxidation, the impedance decreases and the conductivity increases. This confirms well the increase in the peak current obtained for methanol or ethanol oxidation from CV responses shown in Figs. 6 and 7. The results show that the addition of methanol or ethanol causes a decrease in R_{ct} values as shown in Table 2 which demonstrates that R_{ct} and the arc diameter decrease in the following order: Ni/C > Ni–MnO_2/C > Ni–Co_3O_4/C > Ni–ZnO/C > Ni–Fe_2O_3/C in the all studied solutions. The semicircles of the Nyquist plots (Figs. 9, 10 and 11) exhibit different radii, and the smallest radii were recorded for methanol, which suggest that the charge–transfer resistance (R_{ct}) in the case of methanol solution had the fastest electron–charge transfer. In methanol solution, the smallest value of $R_{ct} \approx 6.2\ \Omega\ cm^2$ is obtained with Ni–Fe_2O_3/C and the highest value of $R_{ct} \approx 80.7\ \Omega\ cm^2$ is obtained with Ni–MnO_2/C electrode. The lower R_{ct} confirms that Ni–Fe_2O_3/C is the best electrocatalyst that could improve the catalytic oxidation of methanol or ethanol [94,95]. The small R_{ct} values (Table 2) in methanol or ethanol solution in the presence of Ni–Fe_2O_3/C, Ni–ZnO/C, Ni–Co_3O_4/C and Ni–MnO_2/C suggested a high electron transfer efficiency and a low charge transfer resistance for the studied electrocatalysts, the conductivity increased and consequently a higher electrocatalytic activity was obtained [96]. On the other side, Bode plots for Ni–Fe_2O_3/C, Ni–ZnO/C, Ni–Co_3O_4/C and Ni–MnO_2/C are shown in Fig.11; one distinguishable peak was observed which corresponding to the depressed semicircle in the Nyquist plot. The phase angles (Fig. 11a′–c′) have values less than 90° which confirm the non–ideality of the capacitive behavior of the nanocomposites. In the blank 1.0 M NaOH solution, the phase angle shift had an extra linear part which is attributed to a limited diffusion process [51]. At this potential (E = +0.5 V (MMO)),

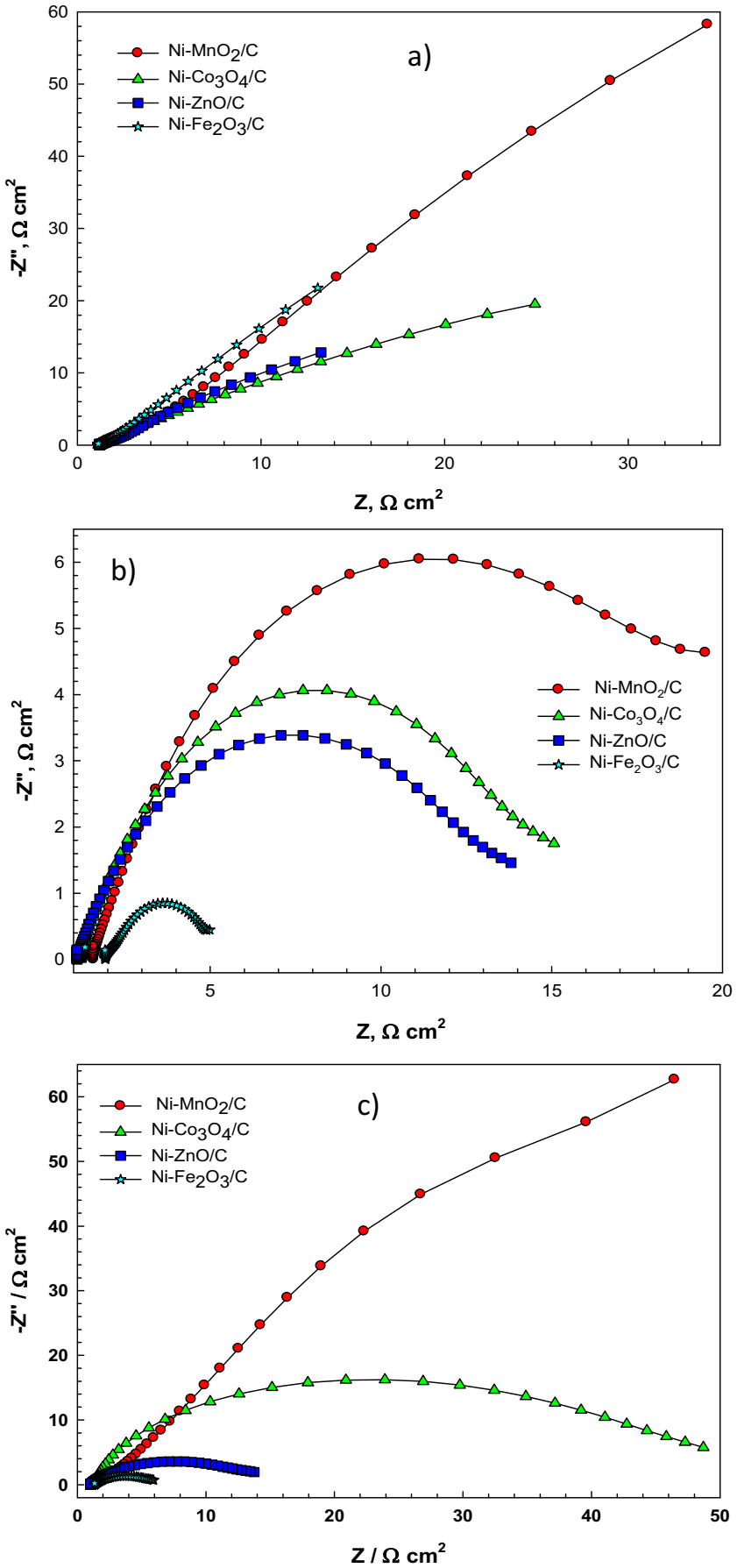

Fig. 10. Nyquist plots of Ni–Fe_2O_3/C, Ni–ZnO/C, Ni–Co_3O_4/C and Ni–MnO_2/C in (a) 1.0 M NaOH solution, (b) 1.0 M methanol and (c) 1.0 M ethanol at +0.5 V (MMO). Symbols denote experimental data, while the continuous lines represent the fitted data.

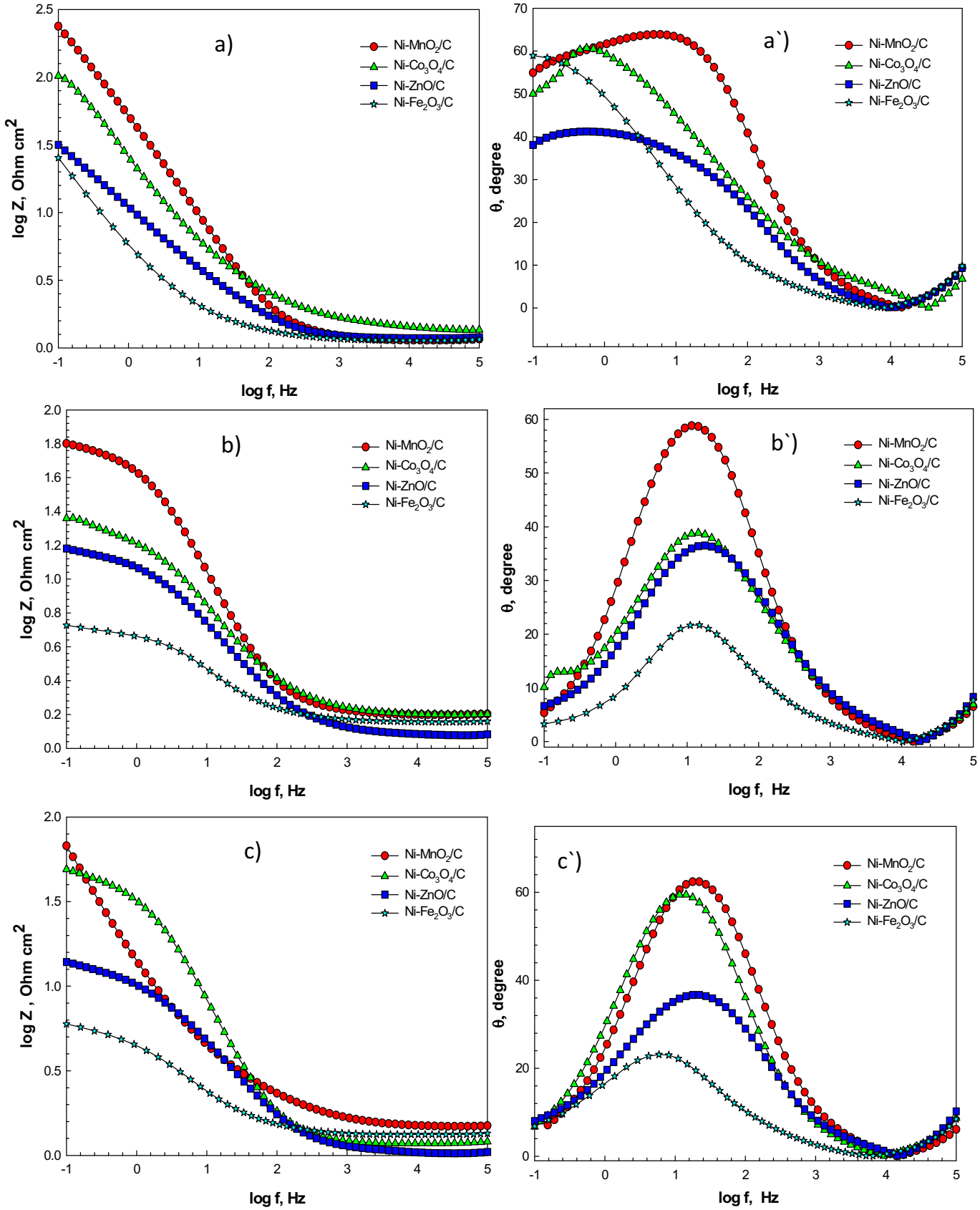

Fig. 11. The impedance and phase angle curves of Ni–Fe_2O_3/C, Ni–ZnO/C, Ni–Co_3O_4/C and Ni–MnO_2/C in (a, a′) 1.0 M NaOH solution, (b, b′) 1.0 M methanol and (c, c′) 1.0 M ethanol at +0.5 V (MMO). Symbols denote experimental data, while the continuous lines represent the fitted data.

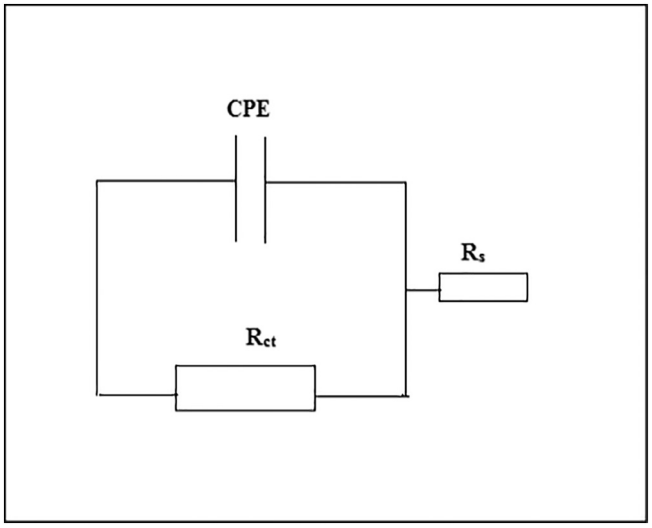

Fig. 12. Equivalent circuit used in the generation of the simulated data for of Ni–Fe_2O_3/C, Ni–ZnO/C, Ni–Co_3O_4/C and Ni–MnO_2/C and Ni/C electrodes prepared at 40 mA cm^{-2} in 1.0 M NaOH and in 1.0 M methanol or 1.0 M ethanol + 1.0 M NaOH solution at a potential value of +0.5 V (MMO).

Table 2
Electrochemical impedance parameters of Ni/C and Ni-metal oxide nanocomposite electrodes in 1.0 M NaOH solution in absence and presence of 1.0 M methanol or 1.0 M ethanol at +0.5 V (MMO).

Electrodes	Solutions	R_s (Ω cm^2)	Q_{dl} (μF cm^{-2})	α	R_{ct} (Ω cm^2)
Ni/C	(a) 1.0 M NaOH	4.8	116	0.70	1129
	(b) 1.0 M MeOH	2.4	639	0.65	106
	(c) 1.0 M EtOH	2.3	458	0.68	158
Ni–MnO_2/C	(a) 1.0 M NaOH	6.16	201	0.65	960.4
	(b) 1.0 M MeOH	3.39	615	0.64	80.7
	(c) 1.0 M EtOH	3.89	591	0.59	250.3
Ni–Co_3O_4/C	(a) 1.0 M NaOH	4.58	347	0.87	318.6
	(b) 1.0 M MeOH	1.23	671	0.64	31.3
	(c) 1.0 M EtOH	1.47	416	0.62	55.4
Ni–ZnO/C	(a) 1.0 M NaOH	5.44	534	0.79	55.1
	(b) 1.0 M MeOH	1.50	982	0.89	15
	(c) 1.0 M EtOH	1.68	830	0.86	19.2
Ni–Fe_2O_3/C	(a) 1.0 M NaOH	5.6	689	0.77	48.4
	(b) 1.0 M MeOH	1.2	836	0.68	6.2
	(c) 1.0 M EtOH	4.3	742	0.74	10.7

oxidation of methanol and ethanol are kinetically (charge–transfer) controlled. It reflects that the electron transfer step during methanol or ethanol oxidation was easier at Ni–Fe_2O_3/C electrocatalyst surface. This confirms that oxidation of methanol and ethanol on the Ni–Fe_2O_3/C is facilitated compared to the other electrodes. Ni–Fe_2O_3/C nanocatalyst provided a high catalytic activity than Ni–ZnO/C which has higher activity than Ni–Co_3O_4/C. The lowest catalytic activity was found for Ni–MnO_2/C. These outcomes were interpreted due to the different oxidation mechanism connected to each catalyst such evidence demonstrates that a multifunctional catalyst may improve methanol or ethanol electrooxidation. This indicates that the variation in the electrocatalytic activity of these nanocomposite catalysts and these results are comparable with that obtained from the CVs of the studied electrodes for methanol and ethanol oxidation. No convection or stirring was done throughout the electrochemical measurements. It is noteworthy mentioning that, five working electrodes were used in all the electrochemical analysis. Different utilization of the electrodes did not affect the performance which supports the good stability of the presented nanocatalysts.

In comparison with the conventional Pt/C catalyst [97,98], the prepared nanocomposites exhibited higher catalytic activities toward electrooxidation of methanol and ethanol. Also, its catalytic activity is more twice than that of the Pt/C electrode (see Table 1). Moreover, its stability towards the electrooxidation process with time is better than that of Pt/C electrode.

.

4. Conclusions

The overall main conclusion is drawing the advantage of using metal oxides to improve the electrocatalytic activity of Ni toward methanol and ethanol oxidation. The nanocomposite electrodes displayed smaller average Ni particle size, better dispersion, higher electrocatalytic activity and better stability. The particle sizes of Ni are 100, 72, 70, 65 and 90 nm for Ni/C, Ni–Fe_2O_3/C, Ni–ZnO/C, Ni–Co_3O_4/C and Ni–MnO_2/C, respectively. The corresponding surface areas are 33, 155, 133, 101 m^2/g for Ni/C, Ni–Fe_2O_3/C, Ni–ZnO/C, Ni–Co_3O_4/C and Ni–MnO_2/C, respectively. Also, Ni-metal oxide nanocomposites improved the kinetic of electron transfer process towards methanol or ethanol electrooxidation compared to Ni/C. Ni–Fe_2O_3/C electrode exhibited the lowest charge transfer resistance values of 6.2 and 10.7 Ω cm^2 for electrooxidation of methanol and ethanol, respectively. Moreover, it gave the highest oxidation peak current densities of 339 and 302 mA cm^{-2} for 1.0 M methanol and 1.0 M ethanol, respectively. The catalytic activity of the different synthesis catalysts was found to be in the order of: Ni–Fe_2O_3/C > Ni–ZnO/C > Ni–Co_3O_4/C > Ni–MnO_2/C > Ni/C. Also, Ni–Fe_2O_3/C showed the highest stability towards the oxidation process over repeated cyclization, its efficiency after 50 cycles was 93% for methanol and 89% for ethanol. It is noteworthy to mention that the Ni–metal oxide nanocomposites are promising candidates for the development of alkaline direct alcohol fuel cells.

References

[1] T. Pardal, S. Messias, M. Sousa, Ana S. Reis Machado, C.M. Rangel, D. Nunes, J.V. Pinto, R. Martins, M. Nunes da Ponte, J. CO2 Utiliz. 18 (2017) 62–72.
[2] G. Hoogers, Fuel Cell Technology Handbook, CRC Press LLC, London, New York, Washington, D.C., 2003.
[3] Zhen-BoWang, Ge-PingYin, Yu-YanShao, Bo-QianYang, Peng-FeiShi, Peter-Xian Feng, J. Power Sources 165 (2007) 9–15.
[4] R. Wang, H. Wang, B. Wei, W. Wang, Z. Lei, Int. J. Hydrog. Energy 35 (2010) 10081–10086.
[5] H. Zhang, Y. Yin, Y. Hu, C. Li, P. Wu, S. Wei, C. Cai, J. Phys. Chem. C 114 (2010) 11861–11867.
[6] W. Zhou, Z. Zhou, S. Song, W. Li, G. Sun, P. Tsiakaras, Q. Xin, Appl. Catal. B Environ. 46 (2003) 273–285.
[7] R. Wang, H. Li, H. Feng, H. Wang, Z. Lei, J. Power Sources 195 (2010) 1099–1102.
[8] Z. Chen, M. Waje, W. Li, Y. Yan, Angew. Chem. Int. Ed. 46 (2007) 4060–4063.
[9] E. Antolini, E.R. Gonzalez, J. Power Sources 195 (2010) 3431–3450.
[10] M. Wang, W. Liu, C. Huang, Int. J. Hydrog. Energy 34 (2009) 2758–2764.
[11] B. Habibi, R. Gahramanzadeh, Int. J. Hydrog. Energy 36 (2011) 1913–1923.
[12] I. Danaee, M. Jafarian, A. Mirzapoor, F. Gobal, M.G. Mahjani, Electrochim. Acta 55 (2010) 2093–2100.
[13] S. Eris, Z. Daşdelen, F. Sen, J. Colloid Interface Sci. 513 (2018) 767–773.
[14] M.A. Scibioh, S.K. Kim, E.A. Cho, T.H. Lim, S.A. Hong, H.Y. Ha, Appl. Catal. B Environ. 84 (2008) 773–782.
[15] C.W. Xua, Z.G. Rong, P.K. Shen, Z.D. Wei, Electrochim. Acta 51 (2005) 1031–1042.
[16] A.M. Jasim, S.E. Hoff, Y. Xing, Electrochim. Acta 261 (2018) 221–226.
[17] S.K. Meher, G. Ranga Rao, ACS Catal. 2 (2012) 2795–2809.
[18] S.K. Meher, G. Ranga Rao, J. Phys. Chem. C 117 (2013) 4888–4900.
[19] X.L. Tong, Y. Qin, X.Y. Guo, O. Moutanabbir, X.Y. Ao, E. Pippel, L.B. Zhang, M. Knez, Small 8 (2012) 3390–3395.
[20] L. Qian, L. Gu, L. Yang, H. Yuan, D. Xiao, Nanoscale 5 (2013) 7388–7396.
[21] M.U. Anu Prathap, B. Satpati, R. Srivastava, Electrochim. Acta 130 (2014) 368–380.
[22] R. Ding, L. Qi, M.J. Jia, H.Y. Wang, Electrochim. Acta 113 (2013) 290–301.
[23] P. Justin, G. Ranga Rao, Int. J. Hydrog. Energy 36 (2011) 5875–5884.
[24] A. Brouzgoua, S.Q. Song, P. Tsiakaras, Appl Catal B 127 (2012) 371–388.
[25] G. Ranga Rao, P. Justin, S.K. Meher, Catal. Surv. Jpn. 15 (2011) 221–229.
[26] H. Huang, X. Wang, J. Mater. Chem. A 2 (2014) 6266–6291.
[27] H. Heli, H. Yadegarib, Electrochim. Acta 55 (2010) 2139–2148.
[28] J.B. Raoof, F. Chekin, V. Ehsani, Bull. Mater. Sci. 38 (2015) 135–140.
[29] S.C. Zignani, V. Baglio, D. Sebastián, S. Siracusano, A.S. Aricò, Electrochim. Acta 191 (2016) 183–191.
[30] H. Rostami, A.A. Rostami, A. Omrani, Electrochim. Acta 194 (2016) 431–440.
[31] C. Xu, P.K. Shen, X. Ji, R. Zeng, Y. Liu, Electrochem. Commun. 7 (2005) 1305–1308.

[32] P.K. Shen, C. Xu, Electrochem. Commun. 8 (2006) 184–188.
[33] R.H. Tammam, M.M. Saleh, J. Electroanal. Chem. 794 (2017) 189–196.
[34] Y. Zhao, L. Zhan, J. Tian, S. Nie, Z. Ning, Int. J. Hydrog. Energy 35 (2010) 10522–10526.
[35] Y. Ren, S. Zhang, H. Li, Int. J. Hydrog. Energy 39 (2014) 288–296.
[36] Z. Wen, S. Yang, Y. Liang, W. He, H. Tong, L. Hao, Electrochim. Acta 56 (2010) 139–144.
[37] C. Xu, P.K. Shen, Y. Liu, J. Power Sources 164 (2007) 527–531.
[38] A. Abdel Aal, H.B. Hassan, M.A. Abdel Rahim, J. Electroanal. Chem. 619 (2008) 17–25.
[39] A. Abdel Aal, H.B. Hassan, J. Alloys Compd. 477 (2009) 652–656.
[40] H.B. Hassan, Z. Abdel Hamid, R.M. El-Sherif, Chin. J. Catal. 37 (2016) 616–627.
[41] J.B. Raoof, N. Azizi, R. Ojani, S. Ghodrati, M. Abrishamkar, F. Chekin, Int. J. Hydrog. Energy 36 (2011) 13295–13300.
[42] F. Chekin, H. Tahermansouri, M.R. Besharat, J. Solid State Electrochem. 18 (2014) 747–753.
[43] F. Chekin, S. Bagheri, A.K. Arof, S.B. Abd Hamid, J. Solid State Electrochem. 16 (2012) 3245–3251.
[44] Y. Wang, Z. Xu, Surf. Coat. Technol. 200 (2006) 3896–3902.
[45] A. Abdel Aal, K.M. Ibrahim, Z. Abdel Hamid, Wear 260 (2006) 1070–1075.
[46] A. Abdel Aal, M. Barakat, R. Mohamed, Appl. Surf. Sci. 254 (2008) 4577–4583.
[47] A. Abdel Aal, Mater. Sci. Eng. A, 474 (2008) 181–187.
[48] M.A. Rahim, R. Abdel Hameed, M. Khalil, J. Power Sources 134 (2004) 160–169.
[49] P.M. Robertson, J. Electroanal. Chem. Interfacial Electrochem. 111 (1980) 97–104.
[50] R.M. Van Effen, D.H. Evans, Electroanal. Chem. Interfacial Electrochem. 103 (1979) 383–397.
[51] R.M. Abdel Hameed, Int. J. Hydrog. Energy 40 (2015) 13979–13993.
[52] J.R. Allen, A. Florido, S.D. Young, S. Daunert, L.G. Bachas, Electroanalysis 7 (1995) 710–713.
[53] T. Shobha, C.L. Aravinda, L. Gomathi Devi, S.M. Mayanna, J. Solid State Electrochem. 7 (2003) 451–455.
[54] P.V. Samant, J.B. Fernandes, J. Power Sources 79 (1999) 114–118.
[55] B. Liu, J.H. Chen, C.H. Xiao, K.Z. Cui, L. Yang, H.L. Pang, Y.F. Kuang, Energy Fuel 21 (2007) 1365–1369.
[56] D.K. Huang, Y.P. Luo, S.H. Li, B.Y. Zhang, Y. Shen, M.K. Wang, Nano Res. 7 (2014) 1054–1064.
[57] J. Xiao, L. Wan, X. Wang, Q. Kuang, S. Dong, F. Xiao, S. Wang, J. Mater. Chem. A 2 (2014) 3794–3800.
[58] R. Ning, J. Tian, A.M. Asiri, A.H. Qusti, A.O. Al-Youbi, X. Sun, Langmuir 29 (2013) 13146–13151.
[59] J. Yu, Y. Ni, M. Zhai, J. Phys. Chem. Solids 112 (2018) 119–126.
[60] A. Abdel Aal, M. Bahgat, M. Radwan, Surf. Coat. Technol. 201 (2006) 2910–2918.
[61] N. Guglielmi, J. Electrochem. Soc. 119 (1972) 1009–1012.
[62] H.B. Hassan, Z. Abdel Hamid, Int. J. Hydrog. Energy 36 (2011) 5117–5127.
[63] R. Xu, J. Wang, L. He, Z. Guo, Surf. Coat. Technol. 202 (2008) 1574–1579.
[64] J. Fransaer, J.P. Celis, J.R. Roos, J. Electrochem. Soc. 139 (1992) 413–425.
[65] H. Lee, J. Jeon, Surf. Coat. Technol. 201 (2007) 4711–4717.
[66] Y. Wu, H. Liu, B. Shen, L. Liu, W. Hu, Tribol. Int. 39 (2006) 553–559.
[67] B.D. Cullity, Elements of X–ray Diffraction, Second ed., Addison Wesley Publishing, London, 1978.
[68] M. Vukovic, J. Appl. Electrochem. 24 (1994) 878–882.
[69] L. Garcıa-Cruz, A. Saez, C.O. Ania, J. Solla-Gullon, T. Thiemann, J. Iniesta, V. Montiel, Carbon 73 (2014) 291–302.
[70] M. Fleischmann, K. Korinek, D. Pletcher, J. Electroanal. Chem. 31 (1971) 39–49.
[71] P. Oliva, J. Leonardi, J.F. Laurent, C. Delmas, J.J. Braconnier, M. Figlarz, F. Fievet, A. de Guibert, J. Power Sources 8 (1982) 229–255.
[72] L. Chen, Y. Tang, K. Wang, C. Liu, S. Luo, Electrochem. Commun. 13 (2011) 133–137.
[73] L. Tang, Y. Li Wang, H. Feng, J. Lu, J. Li, Adv. Funct. Mater. 19 (2009) 2782–2789.
[74] S.T. Nguyen, Y. Yang, X. Wang, Appl Catal B 113 (2012) 261–270.
[75] A. Safavi, H. Kazemi, S. Momeni, M. Tohidi, P. Khanipour Mehrin, Int. J. Hydrog. Energy 38 (2013) 3380–3386.
[76] C. Xu, Z. Tian, P. Shen, S.P. Jiang, Electrochim. Acta 53 (2008) 2610–2618.
[77] L.M. Lu, L. Zhang, F.L. Qu, H.X. Lu, X.B. Zhang, Z.S. Wu, S.Y. Huan, Q. Wang, G.L. Shen, R. Yu, Biosens. Bioelectron. 25 (2009) 218–223.
[78] M. Fleischmann, K. Korinek, D. Pletcher, J. Chem. Soc. Perkin Trans. 2 (1972) 1396–1403.
[79] R.H. Tammam, A.M. Fekry, M.M. Saleh, Int. J. Hydrog. Energy 40 (2015) 275–283.
[80] D. Das, P.K. Sen, K. Das, Electrochim. Acta 54 (2008) 289–295.
[81] D. Das, P.K. Sen, K. Das, J. Appl. Electrochem. 36 (2006) 685–690.
[82] J.-W. Kim, S.-M. Park, J. Electrochem. Soc. 146 (1999) 1075–1080.
[83] J. Lee, D.A. Tryk, A. Fujishima, S.M. Park, Chem. Commun. (2002) 486–487.
[84] J. Frenay, J. Hydrometall. 15 (1985) 243–253.
[85] C. Zhaoy, R. Stanforth, J. Hydrometall. 56 (2000) 237–249.
[86] I.G. Casella, M. Gatta, J. Electroanal. Chem. 534 (2002) 31–38.
[87] D. Das, P.K. Sen, K. Das, J. Electroanal. Chem. 611 (2007) 19–25.
[88] C. Gu, M. Huang, X. Ge, H. Zheng, X. Wang, J. Tu, Int. J. Hydrog. Energy 39 (2014) 10892–10901.
[89] O.O. Fashedemi, K.I. Ozoemena, Electrochim. Acta 128 (2014) 279–286.
[90] P. Bommersbach, M. Mohamedi, D. Guay, J. Electrochem. Soc. 154 (2007) B876–B882.
[91] Z.B. Wang, G.P. Yin, Y.Y. Shao, B.Q. Yang, P.F. Shi, P.X. Feng, J. Power Sources 165 (2007) 9–15.
[92] B. Lu, D. Cao, G. Wang, O. Ga, Int. J. Hydrog. Energy 36 (2011) 72–78.
[93] D.D. Macdonald, Electrochim. Acta 51 (2006) 1376–1388.
[94] R.E. Melinick, G.T.R. Palmore, J. Phys. Chem. 105 (2001) 9449–9457.
[95] A. Döner, E. Telli, G. Kardas, J. Power Sources 205 (2012) 71–79.
[96] N.A.M. Barakat, M.H. El-Newehy, A.S. Yasin, Z.K. Ghouria, S.S. Al-Deyabd, Appl. Catal. A Gen. 510 (2016) 180–188.
[97] P.K. Shen, C. Xu, R. Zeng, Y. Liu, Electrochem. Solid-State Lett. 9 (2006) A39–42.
[98] P.K. Shen, C. Xu, Electrochem. Commun. 8 (2006) 184–188.